www.aem-journal.com

Systematic Approach to Optimize Technological and Economical Aspects of Atmospheric Plasma Sprayed Thermal Barrier Coatings

Jens Igel,* Georg Mauer, Olivier Guillon, and Robert Vaßen

Plasma-sprayed yttria-stabilized zirconia coatings have been used in gas turbines for decades. They are applied for thermal insulation to increase operating temperature and hence efficiency and component's lifetime. To keep manufacturing costs low, especially deposition efficiency is important. However, increasing it is also related to a reduction in porosity, affecting the insulating properties of the layer. To find an optimal combination of efficiency and technological performance, a systematic study of the most affecting parameters of the atmospheric plasma spraying process is conducted, using response surface methodology. In detail, the influence of current, spraying distance, and hydrogen gas flow is investigated with respect to the deposition efficiency, porosity, microstructure, and mechanical properties of the coatings. Characterization is carried out by scanning electron microscopy, microindentation tests, and threepoint bending tests. The models generated based on these measured properties allow predictions of the system responses for any parameter variation in the investigated design space. In addition, a numerical model is developed for targeted optimization of the coating properties. This can be used to produce optimized coatings for load-flexible gas turbines with high deposition efficiency, high porosity, and at the same time advantageous mechanical properties.

J. Igel, G. Mauer, O. Guillon, R. Vaßen
Institute of Energy and Climate Research: Materials Synthesis and
Processing (IEK-1)
Forschungszentrum Jülich GmbH
Wilhelm-Johnen-Straße, 52428 Jülich, Germany
E-mail: j.igel@fz-juelich.de

O. Guillon Jülich Aachen Research Alliance JARA-Energy Wilhelm-Johnen-Straße, 52428 Jülich, Germany

R. Vaßen
Institut für Werkstoffe
Ruhr-Universität Bochum
Universitätstraße 150, 44801 Bochum, Germany

The ORCID identification number(s) for the author(s) of this article can be found under https://doi.org/10.1002/adem.202300623.

© 2023 The Authors. Advanced Engineering Materials published by Wiley-VCH GmbH. This is an open access article under the terms of the Creative Commons Attribution-NonCommercial-NoDerivs License, which permits use and distribution in any medium, provided the original work is properly cited, the use is non-commercial and no modifications or adaptations are made.

DOI: 10.1002/adem.202300623

1. Introduction

Yttria-stabilized zirconia (YSZ) thermal barrier coatings (TBCs) have been used in gas turbines for decades to increase efficiency and improve the component lifetime.[1-3] The most popular manufacturing processes are electron beam physical vapor deposition (EB-PVD) to deposit columnar structured coatings for aerospace turbines and atmospheric plasma spraying (APS) to produce lamellar structured coatings for industrial gas turbines.^[4,5] The columnar structured coatings offer the benefit of a good strain tolerance which is important for load flexibility.^[6] A negative aspect, however, is the reduced thermal insulation due to the dense coating's microstructure.^[7] The advantage of the APS coatings is their good insulation properties, but they are less strain tolerant. [8] A high insulation effect allows operating a gas turbine at high temperatures, making it more efficient. In the future, more load-flexible industrial gas turbines are needed to compensate for the fluc-

tuations in power generation of renewable energies as well as the load fluctuations existing in the power grids.^[9] Fast load changes generate large stresses between the component and the ceramic protective coating due to thermal mismatch, which can lead to coating failure.^[10] Therefore, future coatings for industrial gas turbines need to have higher load tolerance while maintaining their good insulation properties to remain efficient.

The approach in this study is to increase the strain tolerance and durability of the APS coatings by targeted process control. This comprises the optimization of the porosity and mechanical properties of the coatings. Higher porosity not only improves thermal insulation performance, but also reduces the stresses occurring during operation and thus the growth of microcracks.[11] It allows a sliding motion between the flattened particles (splats) forming the coating, which increases the elasticity (lower Young's modulus) of the coating.[12-14] However. increasing porosity negatively affects the process efficiency and thus the coating deposition rates, which are both of great importance in keeping manufacturing times and costs low.[11] Increasing porosity also lowers the coating's hardness, worsening its resistance to erosion wear.^[15,16] This can be explained by the increased degree of irregular porosity and in some cases partially molten particles, which affect the coating's cohesion causing a



ENGINFERING

www.advancedsciencenews.com www.aem-journal.com

tendency to crack propagation. [17,18] Due to these dependencies, an optimal combination of process parameters is required to achieve the goal of an optimized coating for load-flexible gas turbines with high deposition efficiency (DE), high porosity, and advantageous mechanical properties at the same time.

The APS process used is influenced by wide number of parameters, so the most influential parameters on the coating result have to be identified.^[19] In the literature, some parameters are often designated to have a great effect on the results. These are the current [A], the process gas flows [standard liter per minute = nlpm], the spraying distance [mm], the powder feed rate [g min⁻¹], the carrier gas flow [nlpm], and the particle size distribution and morphology. [20-22] To make a suitable trade-off between the process variables, a design of experiment was carried out in this study. With this, many factors as well as their interaction with each other can be investigated and the experimental effort can be reduced. Which type of experimental design is suitable for the specific case depends on several factors. It must be clarified if linear, nonlinear, or quadratic correlations are prevailing. In addition, the number of investigated variables is essential.

Especially, the response surface methodology (RSM), introduced by Box and Wilson in 1951, is an economical and simple method that minimizes the experimental effort.^[23] For this reason, it is used to investigate and optimize processes in various fields of production, research, and engineering.^[24] RSM is a collection of statistical techniques that can be used to achieve different objectives. These include 1) setting up a series of experiments (design) for the determination of the system response, 2) fitting a hypothetical model to experimentally received data, and 3) determining ideal combinations of the model's input variables, to optimize the system response. [25] The independent input (control) variables are considered to span a parameter space for the target value data points to which a mathematical model is fitted. By using a second-order quadratic model, the interactions between the different varied parameters are taken into account. If the RSM is used to optimize the system response by varying the input parameters, the following steps are followed: 1) screening studies to define the area of interest according to the study goal and to identify the independent input variables that have the greatest impact on the system; 2) choosing an experimental design suitable for the study and performing the appropriate experiments; 3) statistical treatment of the generated experimental data by fitting a polynomial function; 4) evaluating the fit of the model; 5) if necessary, optimizing the calculated model; 6) determining the ideal combination of input variables to achieve the optimal system response. [26] The most commonly used types of experimental matrix in RSM are the central composite design (CCD) and the Box-Behnken design (BBD). Details of these can be found in the literature. [23,27] The CCD has five levels for each factor and is an extension of the two-level factorial experimental design. The BBD, on the other hand, has only three levels for each factor and is specifically designed to fit a quadratic model. As the BBD does not examine extreme combinations of all parameters, the prediction is not accurate in the corners of the design space. However, this is compensated by high prediction accuracy in the center of the parameter space, which makes the BBD particularly suitable if the optimal parameter combination for the coating properties is assumed to be located there.

The aim of this study is to combine the APS process parameters, which partly influence each other negatively, in a way to achieve the best possible coating properties. Both the economic aspects of coating manufacturing and the technological coating properties are taken into account. The focus of this work is on pure YSZ powders. The use of YSZ powders with polymeric additives is not considered, as they are more expensive than pure YSZ powders and also require post-thermal heat treatment.

2. Experimental Section

2.1. Developing of the Experimental Design Matrix

The screening pretests of step (1) have shown three particularly influential input parameters for the creation of the design space. It was decided to vary the current between 400 and 500 A, the spraying distance between 160 and 220 mm, and the secondary process gas flow of hydrogen between 5 and 8 nlpm. The primary process gas flow of argon was kept constant at 52 nlpm to analyze the effects of the hydrogen content. At a hydrogen flow rate of 8 nlpm, the argon flow rate led to parameters outside the gun's process window. However, this was done to analyze better the effect of the hydrogen content in the process gas. Within this parameter range, with every combination of the input variables, a coating thickness sufficient for the analysis, as well as desirable deposition efficiencies and porosities could be produced.

In step (2), the BBD was selected as a suitable experimental design matrix for the study as the pretests allowed to suggest the optimal parameter combination for the desired coating properties to be located in the middle of the experimental space. The resulting design matrix is shown in Table 1. This design enables estimation of linear, two-way interactive (two-factor interaction = 2FI), and quadratic effects of the variables on the system responses. A total of seven system responses was analyzed in this study. Besides the DE, the porosity, hardness, and Young's

Table 1. Experimental matrix according to the Box-Behnken design.

Run	Factor 1 (C), current [A]	Factor 2 (SD), spraying distance [mm]	Factor 3 (H), hydrogen [nlpm]	
1	400	190	5	
2	450	190	6.5	
3	450	220	5	
4	450	190	6.5	
5	500	160	6.5	
6	400	220	6.5	
7	450	190	6.5	
8	450	160	8	
9	500	220	6.5	
10	450	220	8	
11	400	160	6.5	
12	500	190	5	
13	400	190	8	
14	500	190	8	
15	450	160	5	

ADVANCED ENGINEERING MATERIALS

www.advancedsciencenews.com www.aem-journal.com

modulus of the coatings were investigated in the as-sprayed state and after a heat treatment. The thermal heat treatment was used to investigate changes in the coating properties during operation. The analysis procedures are described in more detail in Section 2.3.

2.2. Developing Empirical Relationships

In RSM, the relationship between the response variable and the input variables is described by a polynomial equation. The form of the equation depends on the number of input variables and the degree of the polynomial. In total, the system response can be described by the polynomial function as a (curved) plane, called the response surface. In a BBD, the responses of the investigated factors are described in a second-order quadratic model. The mathematical developed model is intended to predict the system responses to parameter variations based on the experimentally measured values. Therefore, the investigated factors are described by functions of the varied plasma spray parameters. The describing functions in this study depend on the current ($x_1 = (C)$), the spray distance ($x_2 = (SD)$), and the hydrogen flux ($x_3 = (H)$), so the system responses are expressed as functions $f(x_i) = f(C)$, (SD), (H)). To describe the effect of a parameter variation and the interaction between the plasma spray parameters, the response surface has to be described with a polynomial. Therefore, Y_i is used to describe the response surface in the following, where i is the number of the investigated system responses. These are coded as i = DE (deposition efficiency), P_a (porosity as-sprayed), HV5_a (Vickers hardness 5N as-sprayed), Ea (Young's modulus assprayed), Pht (porosity heat-treated), HV5ht (Vickers hardness 5N heat-treated), and $E_{\rm ht}$ (Young's modulus heat-treated). The respective response surface Y_i can be described as

$$Y_{i} = Int_{i} + c_{i1}(C) + c_{i2}(SD) + c_{i3}(H) + c_{i12}(C)(SD) + c_{i13}(C)(H) + c_{i23}(SD)(H) + c_{i11}(C)^{2} + c_{i22}(SD)^{2} + c_{i33}(H)^{2}$$
(1)

where Int_i (Intercept) describes the overall average response of all runs. The coefficients $c_{i1}, c_{i2}, c_{i3}, ..., c_{i33}$ represent the expected change in response per unit of the factor value when all other factors are held constant. These coefficients were calculated using Design-Expert 13 statistical design of experiments software. The coefficients can be calculated either in a so-called coded or actual equation. The coded equation allows considering the relative influence of the factors by setting the input factors to +1 or -1) with respect to their maximum or minimum, respectively, and thus normalizing them. The actual equation, on the other hand, can be used with the original units of the parameter. This allows predicting the response at certain levels of each parameter combination. As the factors of the actual equation are not standardized, these factors should not be used to assess their significance.

The experimentally generated data must be processed in mathematical statistical terms following step (3) in order to develop a polynomial function that represents the system response as accurate as possible and with a high level of confidence. The models are generated using the mean values of the measured data. The associated standard deviations can be found in Table S2 and S3, Supporting Information. The empirical relationships were examined in this study by the Design-Expert software using analysis

of variance (ANOVA). This is a statistical technique to compare the average values of the system responses of two or more input variables and to determine their significance. If there are many nonsignificant model terms, reducing by eliminating these factors can improve the model. The quality of the model can be determined by different R^2 values. R^2 is the coefficient of determination showing the fit of the observed data to the regression line calculated by the model. This is calculated by the sum of squares. Adjusted R^2 is a modification of R^2 that takes the number of independent variables into account. It can be used to determine if additional variables contribute to the modeling or if the model is optimized. Predicted R^2 gives a value of the model's ability to forecast new data. This is done by training the model with a subset of existing data and then testing it with the remaining subset of data. To improve the model, an "all hierarchical search" was performed in this study, where the optimization criterion was to maximize the adjusted R^2 . Therefore, results that are due to chance have to be removed from the data. To do this, model terms with a probability of p > 0.1 were removed to exclude nonsignificant terms. Further details on the analysis of variance and tools used in this method, such as the fit summary, the lack of fit test, and others, can be found in the literature. [28] The optimization of the polynomial functions is discussed in detail for each system response investigated in Section 3.

2.3. Materials and Spraying Process

Steel substrates were used with a size of $25 \times 30 \text{ mm}^2$ and a thickness of 2 mm. Before applying the ceramic coatings, the substrates were grit blasted with an F36 Al₂O₃ abrasive to roughen the surface and thus improve the adhesion. The substrates were subsequently cleaned with compressed air and in an ultrasonic bath with ethanol before the ceramic coating was applied timely by APS. The ceramic spray powder used is from Oerlikon Metco with type designation Metco 233C. This agglomerated and sintered powder has a porous structure, which is beneficial for producing porous TBCs. The powder consists of zirconia stabilized with 7-8 wt% yttria which is considered the optimum stabilizer content for TBC applications.^[1] The YSZ was deposited in the t'-phase, which has a high toughness and is stable up to about 1200 °C. [29] However, at higher temperatures, a detrimental phase transformation of the metastable tetragonal t'-phase into the tetragonal and upon cooling in the monoclinic phase occurs. This is associated with a volume expansion of about 5%, generating stresses in the coating leading to failure.[30] Details of the composition of all materials used can be found in Table S1, Supporting Information.

The coatings were applied at Oerlikon Metco in Wohlen, Switzerland on the company's MultiCoat system and at Forschungszentrum Juelich GmbH using an identical system. The two facilities were used because of time reasons. Tests have shown that the same parameters on the identical facilities also produce comparable coating results. Therefore, the use of the different facilities does not influence the result and the results are considered as being produced in one facility. The plasma torch Oerlikon SinplexPro in the 180° version was used. The powder was fed with two 2 mm injectors mounted on the top and bottom of the long injection holder. During the study, the number of passes was adjusted to achieve the desired coating

ADVANCED SCIENCE NEWS ENGINEERING

www.advancedsciencenews.com www.aem-journal.com

thickness of about $500\,\mu m$ with each parameter. The other parameters were kept constant at a feed rate of $100\,g\,min^{-1}$, a meander distance of $4\,mm$, and a robot speed of $1000\,mm\,s^{-1}$.

The heat treatments performed to investigate changes in the coating properties during operation were carried out with free-standing coatings. These were detached electrochemically from the substrate following a procedure described by Vaßen et al. $^{[31]}$ The sintering process was carried out in a furnace under air atmosphere for 100 h at 1200 °C.

2.4. Investigated System Responses

2.4.1. DE

The DE was calculated based on the weight of the deposited coating and describes the percentage of the total powder sprayed that is actually deposited as coating. In addition to the coating weight, the powder feed rate, step width between the meander paths, substrate surface, robot speed, and the number of passes are relevant for the calculation of the DE. This is calculated as given in Equation (2).

$$\begin{split} DE &= \frac{Coating \, weight \, [g]}{\frac{Feed \, rate[g]}{60[s]}} \cdot \frac{Meander \, distance \, [mm]}{Substrate \, surface \, [mm^2]} \\ &\cdot \frac{Robot \, speed \left[\frac{mm}{s}\right]}{Number \, of \, passes} \cdot 100 \, [\%] \end{split} \tag{2}$$

2.4.2. Porosity

Metallographic cross sections were produced to investigate the microstructure and porosity by digital image analysis. They were analyzed using the table top scanning electron microscope TM3000 (Hitachi). Backscattered electron (BSE) images were taken with an accelerating voltage of 15 kV. To determine the porosity values, ten images were taken of each sample at a magnification of 1000 and constant brightness and contrast. The images were taken at randomly distributed locations on the sample. Nonrepresentative areas of the coating damaged during preparation were excluded. The ten representative images were analyzed using the software ImageJ/Fiji. The same Fourier transformation was applied to each image to sharpen it. Afterward, the threshold was set manually to capture all relevant pore areas. Applying this threshold, the grayscale images were converted into binary images on which the porosity values are determined. The mean value of the ten images is then taken as the porosity value for the parameter combination used.

2.4.3. Hardness

The hardness values were determined using the Struers Duramin A300 hardness tester. The investigation was performed with a Vickers indenter on the same polished cross sections used for the porosity analysis. The mean value was again calculated from ten measurements taken in the center of the coating in intervals of 2 mm (about 1.2 mm on the heat-treated freestanding coatings). The microindentation tests were performed with a test load of 5 N. The Vickers hardness [HV] of the coatings was determined based on the size of the indent. The high test force and resulting large

indentation helped to avoid a high variation in the measurement results, as the global hardness of the coating was determined.

2.4.4. Young's Modulus

Three-point bending tests were used to determine the timedependent elastic stress capacity and stress relaxation of freestanding coatings at room temperature. Therefore, rectangular samples with a length of 15 mm and a width of 4 mm were cut out of free-standing coatings using a diamond saw. The coatings were detached electrochemically as described by Vaßen et al. [31] The exact thickness of each sample, which was kept uniform by adjusting the number of passes to the coating parameters, was determined using the CT 350T profilometer from Cyber Technologies via a double-sided measurement with a chromatic white light sensor. The elastic properties and viscoplastic deformation of the free-standing coatings were investigated in the TMA dilatometry facility Setsys TMA-18 of the company Setaram Inc. The experimental setup is shown schematically in Figure 1a. The distance between the support points (*L*) is 12 mm. Four loads (F) (15, 30, 45, 60 g) were applied successively to each specimen and held for 30 s each. Between the loadings, the duration for stress relaxation was also increased (60, 120, 180, 240 s). At least five bending samples were tested for each spray parameter, and an average value was calculated from the measurement results.

The evaluation was done by fitting the Burger's model to the data as described in the literature. [14] The deformation (δ) of the specimen was measured continuously. A schematic of such a strain curve is shown in Figure 1b. During the application of the load $(t_1 \text{ to } t_2)$, elastic deformation of the coating occurs. After reaching the maximum load, the load is kept constant (t_2 to t_3). During this time, viscous creep (vc) of the ceramic takes place due to splat sliding, so the deformation increases further. When the specimen is unloaded $(t_3 \text{ to } t_4)$, the elastic response decreases again. In addition, there is a partial recovery of creep after the removal of the load (after t_4). Nevertheless, a residual displacement remains at the end (t_5) , called viscoplastic deformation (vd). The calculation of the Young's modulus was made using the displacement during unloading $\delta(t_4 - t_3)$ to exclude the influence of creep during the loading period. As different loads were applied during the measurement, the force-displacement relationship was taken as the slope of the force-displacement function assuming it as linear. The Young's modulus could then be calculated using Equation (3). The geometric factor λ is described by the specimen's width (b) and height (h) and the distance (L) between the support pins.

$$E = \frac{F}{\lambda} \cdot \frac{1}{\delta(t_4 - t_3)}, \quad \lambda = \frac{4bh^3}{L^3}$$
 (3)

3. Results and Discussion

3.1. Models to Predict System Responses

The Design-Expert software was used to create models to predict system responses. First, the fit summary of the system responses was considered. This proposes a model design based on the calculated Whitcomb Score, which provides a good starting point

15272648, 2024. 4, Downloaded from https://onlinelibrary.wiley.com/doi/10.1002/adem.202300623 by Forschungszentrum Jülich GmbH Research Center, Wiley Online Library on [11.03/2024]. See the Terms

on Wiley Online Library for rules of use; OA articles are governed by the applicable Creative Commons

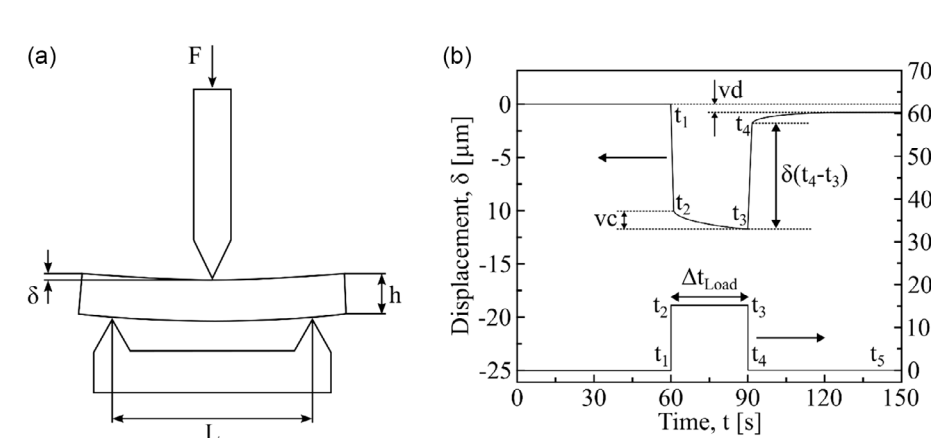


Figure 1. a) Schematic setup of three-point bending test in TMA facility; b) typical progression of loading with time and the resulting viscoelastic/visco-plastic response of the material to in-plane strain.

for model fitting. The Whitcomb Score is a heuristic scoring system calculated based on the sequential p-values of the model, the lack of fit, and the predicted and adjusted R^2 . The model achieving the highest score serves as a starting point for the model fitting. Afterward, the "all hierarchical search" was used for the model. In this search, the adjusted R^2 is maximized and nonsignificant terms with p > 0.1 were removed. These steps were initially performed on all models. Further adjustments of the models of the system responses are explained in more detail in the following sections.

3.1.1. DE

The fit summary proposed a quadratic model to calculate and predict the DE. Using the all hierarchical search, the model term (SD)·(H) was removed, as it is not significant with a p-value > 0.1. All other terms are significant with p < 0.05. In **Table 2**, the

ANOVA of the reduced quadratic model is shown. The F-value of the model is statistically significant, meaning it is unlikely that the observed differences between the individual parameters are due to chance. The probability of an F-value this large, being due to noise is less than 0.01%. This allows us to conclude the effects observed in the model are true and are not due to random fluctuations. The fitted model has a coefficient of determination (R^2) of 0.9911, which means the model fails to explain only 0.89% of the total variation, but 99.11% of the experimental data is predicted by the model. Furthermore, the predicted R^2 of 0.9141 agrees well with the adjusted R^2 of 0.9792, as the difference is less than 0.2, which is desirable.

$$Y_{DE}^{Coded} = 48.47 + 13.11(C) - 8.34(SD) + 5.78(H)$$

$$+ 3.91(C)(SD) - 5.29(C)(H) - 6.74(C)^{2}$$

$$- 6.02(SD)^{2} - 2.72(H)^{2}$$
(4)

Table 2. ANOVA test results for DE with df: degrees of freedom; CV: coefficient of variation; F: Fisher ratio; and p: probability.

Source	Sum of squares	df	Mean square	F-value	p-value prob $> F$	Significant
Model	2663.43	8	332.93	83.58	< 0.0001	Significant
(C)—Current	1374.45	1	1374.45	345.06	< 0.0001	
(SD)—Spray distance	556.44	1	556.44	139.70	< 0.0001	
(H)—Hydrogen flow	266.81	1	266.81	66.98	0.0002	
(C) (SD)	61.07	1	61.07	15.33	0.0078	
(C) (H)	111.83	1	111.83	28.08	0.0018	
(C) ²	167.96	1	167.96	42.17	0.0006	
(SD) ²	134.01	1	134.01	33.64	0.0012	
(H) ²	27.41	1	27.41	6.88	0.0394	
Residual	23.90	6	3.98			
Lack of fit	17.96	4	4.49	1.51	0.4353	Not significant
Pure error	5.94	2	2.97			
Cor total	2687.32	14				
SD = 2.00			$R^2 = 0.9911$			
Mean = 40.20		Ad	j. $R^2 = 0.9792$			
CV% = 4.96		Pre	d. $R^2 = 0.9141$			
PRESS = 230.80		Adeq. p	precision = 28.1317			

ditions) on Wiley Online Library for rules of use; OA articles are governed by the applicable Creative Commons

ADVANCED ENGINEERING

www.aem-journal.com

www.advancedsciencenews.com

$$\begin{split} Y_{DE}^{Actual} &= -864.316 + 2.654(C) + 1.093(SD) + 51.317(H) \\ &+ 0.003(C)(SD) - 0.071(C)(H) - 0.003(C)^2 \\ &- 0.007(SD)^2 - 1.211(H)^2 \end{split} \tag{5}$$

The coded and actual equations presented in Section 2.4 (Equation (1)) can be used to predict effects by the calculated model. For the DE, the coded Equation (4) can be used, inserting values from -1 to 1 for the parameters in the design space. This allows evaluating the variables' relative influence on the system response. The equation shows the current has the largest influence on DE. It is followed by the spraying distance and finally the hydrogen content. The F-values of the ANOVA as well support this conclusion. The influence of the 2FI and quadratic factors can also be seen in Equation (4). It is known that a higher arc current creates more power, increasing the specific enthalpy and temperature of the plasma. With increasing temperature, the plasma's density decreases, increasing its velocity.[32] Similarly, the plasma's specific enthalpy, temperature, and velocity are increased by adding more hydrogen to the plasma.^[33] Furthermore, the specific heat capacity and the thermal conductivity of the plasma rise. This favors transferring the energy stored in the plasma to the injected powder and consequently its melting. $^{[11]}$ The higher ratio of molten particles leads to an increase in efficiency. The lower DE at higher spraying distances can be explained as the particles are only heated and accelerated in the plasma on the first few centimeters toward the sample. After that, they cool down again and are slowed down. [34] As a result, some particles resolidify and bounce off the sample, reducing efficiency. Also, the particle plume expands with higher standoff distance causing some particles not to hit the substrate. The actual Equation (5), on the other hand, shows how the result is calculated when using the actual parameter values with units. The response surface described by this Equation (5) is shown in Figure 2a.

3.1.2. Porosity

A linear model was proposed for porosity analysis based on the Whitcomb Score. From this model, no term was removed after the all hierarchical search. Even though the spraying distance with a *p*-value of 0.4002 had no significant influence on the

porosity for the investigated design space, it remains in the model to always be able in future to analyze the effect of all input parameters. The nonsignificant effect of the spraying distance on the porosity becomes visible by looking at the model's response surfaces in Figure 2b. The isocontour lines on the base plane of the cube for the porosity are almost parallel to the axis of spraying distance. One possible cause is that small particles resolidify at a high standoff distance and do not deposit in the coating. This would also explain the drop in efficiency. To porosity, these small particles did not contribute at a low distance as they were molten. The large particles, on the other hand, maintain sufficient temperature and kinetic energy even at higher distances. Therefore they flatten to a similar degree, resulting in a comparable porosity. Nevertheless, the linear model used to describe the porosity response is significant and the lack of fit test is not significant compared to the pure error. Thus, no significant patterns in the residuals cannot be explained by chance. The three R^2 values also show that the model can be used to predict the system's behavior.

The *F*-values from the ANOVA (further ANOVA tables are in the Appendix in Table S4–S9, Supporting Information) and the coded Equation (6) show the most considerable influence on porosity by changing the current.

As described in Section 3.1.1, the velocity and temperature of the plasma increase with a higher current. This is transferable to the particles. Due to the particle's higher kinetic energy and temperature, there is a wide spread of the droplets on impact. Besides the improved efficiency, this also leads to a densified, less porous coating.^[35]

$$Y_p^{\text{Coded}} = 20.03 + 5.39(\text{C}) + 0.60(\text{SD}) - 2.48(\text{H})$$
 (6)

3.1.3. Hardness

In the hardness analysis, the fit summary yields the highest score for the quadratic model. This was then reduced by the all hierarchical search and the model terms $(C) \cdot (SD)$, $(C)^2$, and $(SD)^2$ were removed, as their influence on the model is not significant. Based on the regression Equation (7) as well as the *F*-values, it can be concluded that the spraying distance has the smallest influence on the hardness. But in contrast to the porosity model, the

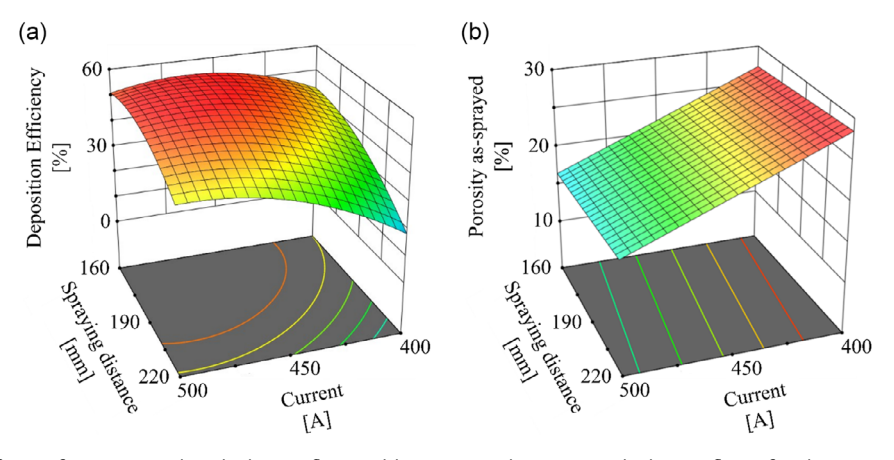
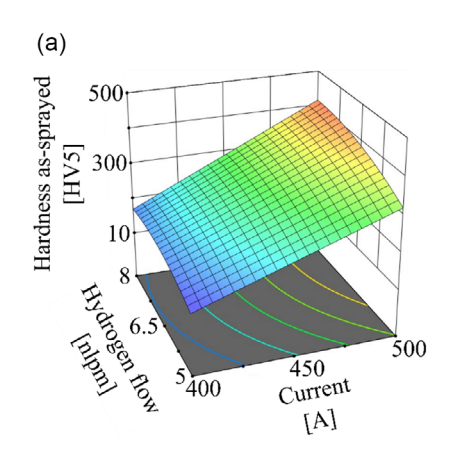


Figure 2. Response surfaces of a) DE at 8 nlpm hydrogen flow and b) as-sprayed porosity at hydrogen flow of 5 nlpm.

nditions) on Wiley Online Library for rules of use; OA articles are governed by the applicable Creative Commons



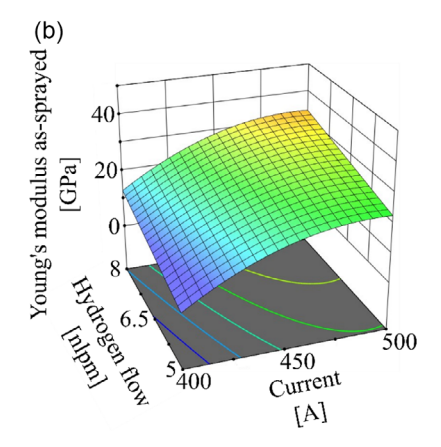


Figure 3. Response surfaces in the as-sprayed state of a) hardness at 220 mm spraying distance and b) Young's modulus at 220 mm spraying distance.

spraying distance has a significant influence. The strongest impact on the hardness is again the current intensity used. The effects leading to the lower porosity result in an increase in hardness.^[21] As the lack of fit test and the fit statistics show, this model is also suitable for predicting the system behavior in the investigated parameter space. The corresponding plotted response surface can be found in Figure 3a.

$$Y_{\text{HVS}_{as}}^{\text{Coded}} = 299.64 + 107.49(\text{C}) - 14.90(\text{SD}) + 41.62(\text{H}) + 15.61(\text{C})(\text{H}) - 9.38(\text{SD})(\text{H}) - 23.49(\text{C})^2$$
(7)

3.1.4. Young's Modulus

The fit summary calculation proposed a linear and a quadratic model for calculating the regression model to predict Young's modulus from the three-point bending tests. The reason for this is, there are always two Whitcomb Scores calculated. One using the predicted R^2 and one using the adjusted R^2 . If different models score the highest on the two scores, they are both suggested. However, the lack of fit of the linear model is significant compared to the pure error. It can be concluded that there are significant patterns in the residuals that cannot be explained by chance and that the regression model is insufficient to describe the relationship between the variables. A poor fitting model can lead to inaccurate predictions and incorrect conclusions. In such a case, additional factors should be investigated or a higher order model should be used. This is possible with the quadratic model. The all hierarchical search removes the model terms (C)·(SD), (C)·(H), (SD)·(H), and (H)² from the quadratic model as they are insignificant. The nonsignificant model term (SD) remains in the model as otherwise, the model would not be hierarchical. One or more terms of higher order would be included in the model regarding (SD), but the supporting lower order term (SD) itself would not be included. The ANOVA table calculated from this shows the model is significant, the lack of fit is not significant, and the difference between predicted and adjusted R^2 is less than 0.2. Therefore, this model can also be used to predict the system responses. The main influence on the system response is again the current (Equation (8)). As explained for porosity, the particles flatten less with lower current, having a lower temperature and

kinetic energy on impact. At the less flattened droplets, stresses are focused, leading to crack propagation in multiple directions, resulting in a reduced elastic modulus.[21,36]

$$Y_{E_{as}}^{\text{Coded}} = 30.77 + 10.10(\text{C}) - 0.73(\text{SD}) + 5.26(\text{H}) - 6.00(\text{C})^2 - 6.11(\text{SD})^2$$
(8)

Accordingly, step (4) of the procedure for an RSM is completed and the fit of all models is evaluated. As all models fit for making predictions, step (5) can be skipped, as no optimization is necessary. The corresponding plotted response surface can be found in Figure 3b.

3.2. Correlations between System Responses in the **As-Sprayed State**

In Section 3.1, the process parameters' effect on the system responses was considered. However, it already became visible that there is a strong correlation between the system responses, which will be investigated in more detail in this section. The linear correlations between the system responses can be found in **Table 3**. The lowest correlation is between the DE and Vickers hardness. This value is 0.812, which still indicates a strong correlation. Understanding and controlling the relationships between the system responses is of great importance to find system responses that meet the required demands. This is especially relevant for factors that influence each other in an unwanted manner, such as decreasing porosity with increasing DE.

Table 3. Linear correlations between system responses.

	DE_{as}	P_{as}	HV5 _{as}	E _{as}	P_{ht}	HV5 _{ht}	$E_{\rm ht}$
DE_{as}	1.000	-0.822	0.812	0.823	-0.784	0.761	0.757
P_{as}		1.000	-0.932	-0.903	0.877	-0.838	-0.738
$HV5_{as}$			1.000	0.816	-0.817	0.784	0.702
E_{as}				1.000	-0.905	0.876	0.757
$P_{\rm ht}$					1.000	-0.925	-0.605
$HV5_{ht}$						1.000	0.575
$E_{\rm ht}$							1.000

iditions) on Wiley Online Library for rules of use; OA articles are governed by the applicable Creative Commons

www.advancedsciencenews.com

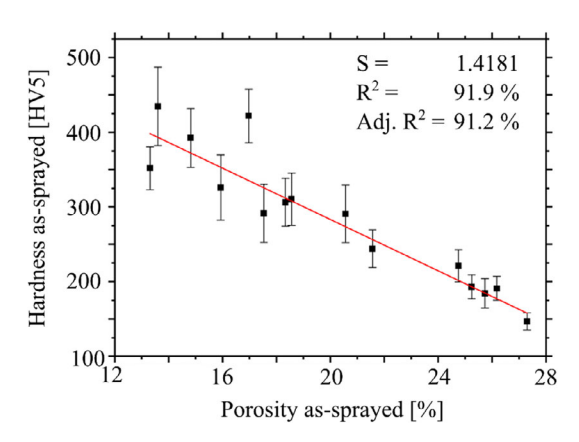


Figure 4. Relationship between porosity and Vickers hardness in the as-sprayed state.

In interpreting the system responses, porosity was related to the mechanical properties of the coatings. The correlation between porosity and Vickers hardness of -0.932 is the strongest in the entire study. In addition, the correlation between porosity and Young's modulus is also strong at -0.903. These correlations between the microstructural and mechanical properties are also known from literature. [15,21] As shown in Figure 4, the coating's hardness decreases nearly linearly with increasing porosity. This is because cracks propagate more easily at existing microcracks and pores. Under load, stress peaks are generated at these points, which lead to crack propagation. This effect is even increased as stresses are not distributed equally in the inhomogeneous coating.^[37] Furthermore, viscous creep occurs between poorly bonded splats under load, which reduces the hardness values. [14] Also, the large indentation volume leads to more pores and cracks being hit, which reduces the coating hardness. The slope of the regression line has the value -17.1862 HV5 with a standard deviation (S) of ± 1.4181 . Thus, the straight line can be described by the regression Equation (9). The fitted regression line can be used to estimate the mean value of the coating's hardness for a given value of coating porosity.

$$Hardness_{as-sprayed}[HV5] = 626.96 - 17.1862 \cdot (Porosity in vol\%)$$

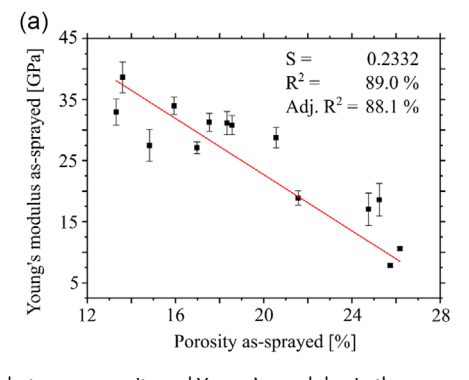
A comparable behavior is found in the analysis of the threepoint bending tests as the Young's modulus also decreases with higher porosity, as shown in Figure 5a. The numerous pores and microcracks weaken the structure and reduce the material's effective cross-sectional area, reducing the stiffness.^[21] Another effect reducing the Young's modulus is the sliding between poorly bonded splats and along defects. This viscoplastic deformation can also be seen in the force-displacement curves of the bending tests in Figure 5b. Under constant load, the displacement increases significantly more for the porous specimens due to creeping. The viscosity can be calculated from the tangential slope of the strain curve under constant load. This is dependent on the strain rate during creep. Details of the calculation can be found in Ahrens et al. [14] In this study, it was shown that a creep duration of 15 min was not sufficient to achieve a constant strain rate at room temperature. Therefore, the evaluation of creep in this study was carried out only graphically due to the large sample volume. The estimation of the Young's modulus by porosity can be made using the equation given in formula (10).

Young's modulus_{as-sprayed} [GPa] =
$$68.67 - 2.2986$$

 \cdot (Porosity in vol%) (10)

3.3. Influence of Heat Treatment on Coating Properties

Up to now, only the properties of the coatings in the as-sprayed state have been analyzed. However, they change under the high temperatures which the TBCs experience during operation in a turbine. Therefore, the porosity, hardness, and Young's modulus were also investigated after heat treatment to simulate the sintering of the coating in service. The same procedure as for the as-sprayed analyses was followed to generate the models for prediction. The corresponding ANOVA and regression equations from this section can also be found in the Appendix. After the 100 h heat treatment at 1200 °C, a reduced quadratic model was generated to predict both porosity and Vickers hardness. The highest influence on the results has again the current. This is also the case for the Young's modulus of the heat-treated coatings. However, this system response is described with a 2FI model, with additional linear interactions between two parameters at a time. As with the as-sprayed coatings, there is a strong correlation between the properties of the heat-treated coatings (Table 3). The strongest correlation after heat treatment remains between porosity and hardness (-0.925). The dependence



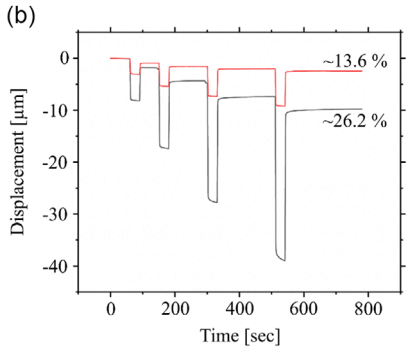


Figure 5. a) Relationship between porosity and Young's modulus in the as-sprayed state; b) force—displacement curves from three-point bending tests for different porosity levels.

ADVANCED ENGINEERING MATERIALS

www.advancedsciencenews.com www.aem-journal.com

between porosity before and after heat treatment is also high (0.877).

The changes observed in the models can be explained by sintering processes during heat treatment. These cause microcracks and pores in the ceramic to close and the interlamellar bond is strengthened. As a result, the porosity in the coatings decreases, which reduces the insulating performance of the TBC and increases the hardness and Young's modulus of the densified coatings.^[38] The heat treatment increased the hardness in the layers by about 75 HV5 on average. The rise in hardness is higher in the previously denser and harder coatings, with an increase of more than 125 HV5. For the more porous and softer coatings, the raise in hardness is only about 25 HV5. A comparison of the microstructures before and after sintering is shown in the following Figure 6. The more considerable increase in the denser coatings is explained by decreasing porosity and healed microcracks (compare Figure 6a,b). At a higher porosity, only fine cracks and small pores are closed. The areas with unmelted fractured particles and large defects still remain after heat treatment (compare Figure 6c,d). Thus, a lot of porosity is still covered by the indentation, which is why the global hardness increases only slightly after heat treatment.

The expected trend was observed for the bending samples, but the correlation between porosity and Young's modulus was weaker with a value of -0.605. This can be seen in **Figure 7a**. On average, the Young's modulus increased by 29 GPa due to the heat treatment and sintering. Notably, the range before heat treatment was between approximately 8 and 39 GPa and after sintering between 39 and 76 GPa. Many coatings almost doubled their stiffness during sintering. This is consistent with the results of Ahrens et al. $^{[14]}$ But the very porous layers in particular

received a significant increase in hardness from sintering, contrary to the hardness measurements. The previously softest samples, for example, have a hardness increase from about 8 to 42 GPa and about 11 to 39 GPa. Therefore, it can be assumed that the sintering of fine cracks and pores will prevent a sliding within the layer during deformation, significantly influencing the Young's modulus. This is also reflected in the decrease in viscoplastic creep after heat treatment (Figure 7b,c). However, it should be noted that the samples were sintered as free-standing coatings. This leads to stronger sintering than for coatings applied on a substrate.^[39]

3.4. Optimization of Coatings Properties Using Generated Models

In the previous section, the effects of the parameters on the system responses were considered based on the generated models and it was analyzed how the system responses relate to each other. As these partially influence each other in an undesirable way, a tradeoff must be found during parameter optimization to achieve the best performance of the TBC. For instance, an increase in porosity improves insulation performance and decreases stiffness, which benefits the efficiency and durability of the coating in service. However, it also lowers hardness and DE in the manufacturing process, which is disadvantageous. Higher hardness protects the coating from erosive wear, and high DE is important from an economic point of view to enable time-efficient and thus cost-effective production of the components.

The final step (6) of the RSM to determine the optimum coating parameters was also performed using Design-Expert

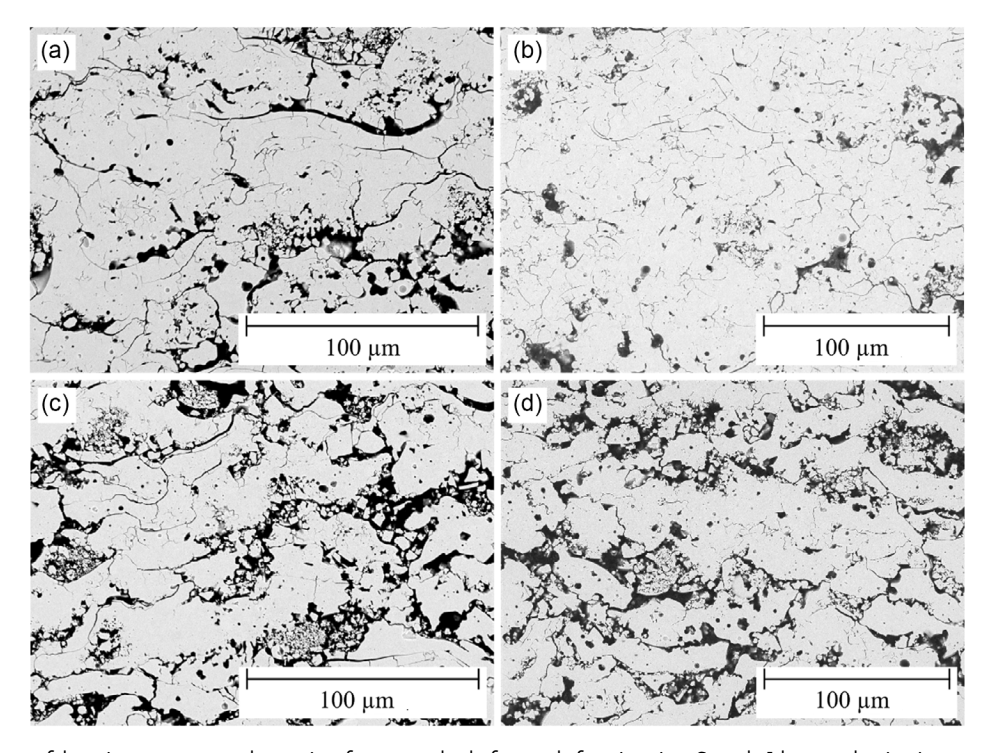


Figure 6. Comparison of the microstructure and porosity of two samples before and after sintering. Sample 1 has a reduction in porosity from a) 18.3% to b) 12.5% and sample 2 from c) 25.7 to d) 22.4%.

szentrum Jülich GmbH Research Center, Wiley Online Library on [11/03/2024]. See the Terms and Conditions

ditions) on Wiley Online Library for rules of use; OA articles are governed by the applicable Creative Commons

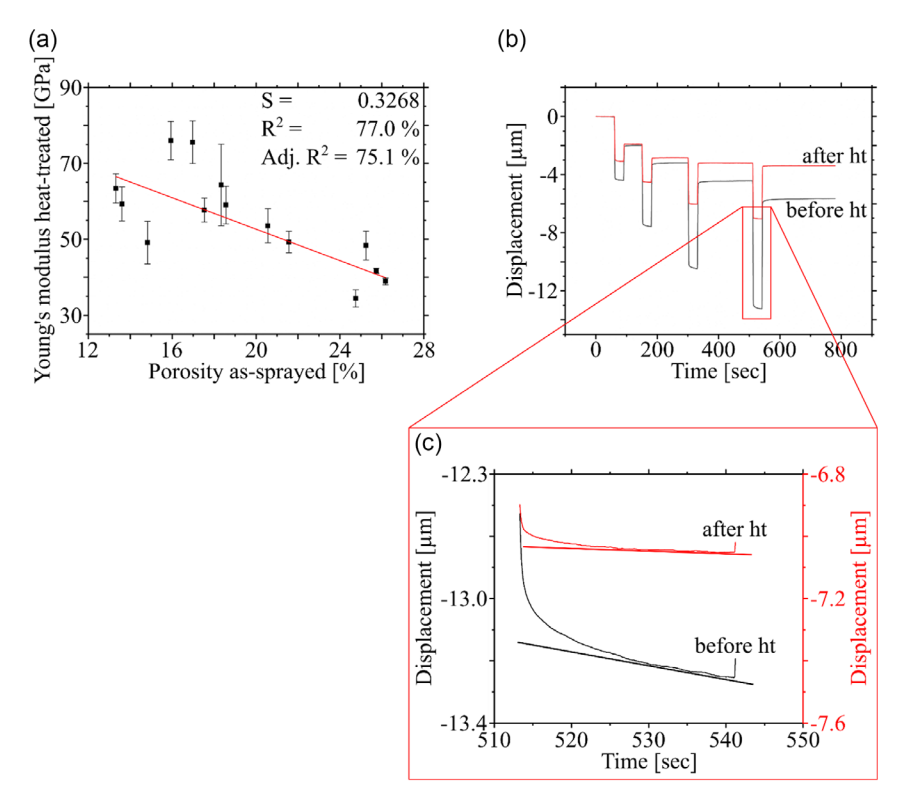


Figure 7. a) Relationship between porosity and Young's modulus in the heat-treated state; b) force—displacement curves from three-point bending tests of samples sprayed with the same parameter before and after heat-treatment with c) a zoom in.

software. The numerical optimization module was used. This uses the generated models to search in the factor space for the best tradeoffs. A goal is given for each input variable and each system response. Possible objectives include maximize, minimize, target, and in range. In addition, a minimum and maximum value achievable must be specified for the input variables and system responses to define the range of search for the optimum. The last step for numerical optimization is to assign a relative "importance" to the objectives, which is used to determine their relative importance. It is possible to choose between the values 1-5, where 5 describes a critical goal with the highest priority, 1 a goal of low importance, and 3 is considered as a standard value of medium priority. The defined goals are combined to a general desirability function. The software attempts to maximize this function. The starting points of the calculation are the points of the experimental design and random starting points. The target search leads to a (local) maximum over the steepest slope.

For the numerical optimization, the target "in range" was selected for the input variables current and spraying distance. The search for the optimum parameters takes place in the entire design space between 400 and 500 A and between 160 and 220 mm. To always keep the process within the operating window of the torch, the upper limit of the third input variable, the hydrogen flow, was lowered from 8 to 6.5 nlpm. For the system responses, the upper and lower system limits are defined by the maxima and minima occurring in the individual models. The system responses being maximized in the optimization are DE as well as porosity and hardness in the as-sprayed state

and after heat treatment. The modulus of elasticity in the assprayed state and after heat treatment is minimized. The standard value of 3 was also used for the importance of most of the targets. Only the importance of the two porosity goals was set to the highest value of 5 because porosity has shown the highest influence on the mechanical properties and being the crucial factor for the thermal insulation and thus the efficiency of the coating in operation. The DE, on the other hand, was downgraded to the lowest importance with a value of 1 because the main focus is on the generation of a long-lasting coating in operation. In addition, the economic efficiency of the process is ensured by the high feed rates used, which keep the processing

Table 4. Constraints in search of the optimal coating parameters.

Name	Goal	Lower Limit	Upper Limit	Importance
(C)	In range	400	500	3
(SD)	In range	160	220	3
(H)	In range	5	6.5	3
DE	Maximize	10.51	54.17	1
P_{a}	Maximize	13.31	27.29	5
HV5 _a	Maximize	146.744	434.687	3
Ea	Minimize	7852	38.612	3
$P_{\rm ht}$	Maximize	12.52	26.09	5
HV5 _{ht}	Maximize	174.548	559.436	3
$E_{\rm ht}$	Minimize	34.438	76.042	3

and-conditions) on Wiley Online Library for rules of use; OA articles are governed by the applicable Creative Commons

www.advancedsciencenews.com www.aem-journal.com

Table 5. Validation of the models by comparing predicted and actually achieved system responses in the as-sprayed state.

Sample	Current	Spray distance	Hydrogen	DE [%]		Porosity [%]		Hardness [HV5]	
	[A]	[mm]	[nlpm]	Predicted	Actual	Predicted	Actual	Predicted	Actual
Val-2	411	161	6.5	39.52	42.24	23.65	$\textbf{24.18} \pm \textbf{1.78}$	230.21	221.01 ± 22.65
Val-3	411	161	6.2	37.43	40.70	24.15	$\textbf{24.49} \pm \textbf{1.55}$	221.57	214.01 ± 13.14
Val-4	447	219	5	24.92	28.16	23.24	$\textbf{25.55} \pm \textbf{2.22}$	223.69	194.18 ± 22.09
Val-5	430	160	5.3	37.97	39.94	23.57	$\textbf{23.64} \pm \textbf{2.16}$	220.72	220.30 ± 14.33
Val-6	414	209	6.1	23.30	23.50	24.95	$\textbf{27.06} \pm \textbf{2.28}$	204.63	201.41 ± 15.14
Val-7	411	161	6.2	37.43	39.68	24.15	$\textbf{24.40} \pm \textbf{2.52}$	221.57	$\textbf{232.50} \pm \textbf{27.33}$

times low. These parameters set for the optimization are summarized in Table 4.

From the 9 parameter combinations investigated in the new defined design space as well as 100 randomly selected starting points, the numerical search for local maxima of the desirability function was started. Nine parameter combinations were found to optimize the desired system responses in combination. Of these parameter combinations, five different ones were sprayed to validate the model. The predicted and actually achieved system responses in the as-sprayed state can be found in Table 5. The validated values of the as-sprayed system responses have a good agreement with the predicted values as these are within the 95% confidence interval. This indicates the model is well suited for predicting the system responses in the defined parameter space. These results with a uniform importance of all factors of value 3 deviate only slightly from these predictions. In this case, the predicted optimum value has an efficiency of 41.4%, a porosity of 23.0% percent, and a corresponding hardness of about 243 HV5. The production parameters are also comparable with 420 A current, a standoff distance of 160 mm and a hydrogen flow of 6.3 nlpm. The small deviation in the prediction with different importance of the factors is related to the high influence of porosity on the mechanical properties. As a result, these combined influence the model more than the DE. Thus, the model can be used to specifically adjust the spray parameters according to desired coating properties. However, it should be emphasized that the calculated models are only valid for the torch and material used in the study. Similar products, nevertheless, will show comparable tendencies. The approach of the RSM, however, is common and can be transferred to similar studies.

4. Conclusion

The APS parameters (current, spraying distance, and hydrogen flow) were optimized to maximize the performance of TBCs. Multiresponse optimization with RSM was performed to produce YSZ coatings with maximum porosity, hardness, and DE combined with minimum Young's modulus. The results were used to create empirical relationships between input parameters and coating properties. The main findings are as follows: 1) The current intensity has the largest influence on DE and the coating properties. 2) The spraying distance has no significant effect on the porosity and the mechanical properties in the investigated

design space. 3) There is a strong correlation between porosity and mechanical properties.

Based on these findings, mathematical functions were generated to predict each system response for an arbitrary combination of parameters in the design space. In addition, equations were developed to estimate the mechanical properties based on the porosity values. Finally, a model has been created that predicts parameter combinations for producing the optimal coating properties desired by its user.

Supporting Information

Supporting Information is available from the Wiley Online Library or from the author.

Acknowledgements

This work is part of the LaBeGa project, which was funded by the Federal Ministry of Economic Affairs and Climate Action (BMWK), Germany, within the framework of the 7th Energy Research Program (FKZ 03EE5045A). In addition, the authors would like to thank the project partner Oerlikon Metco WOKA GmbH for performing experiments and providing materials. Furthermore, the authors would like to thank the following colleagues of the institute for their support: Mr. Karl-Heinz Rauwald, Mr. Frank Kurze, and Mr. Ralf Laufs for the plasma spray coating of the samples as well as Dr. Hanna Heyl and Dr. Robert Mücke for their support with the three-point bending tests.

Open Access funding enabled and organized by Projekt DEAL.

Conflict of Interest

The authors declare no conflict of interest.

Data Availability Statement

The data that support the findings of this study are available in the supplementary material of this article.

Keywords

atmospheric plasma spraying, Box–Behnken design, economic efficiency, mechanical properties, response surface methodology, thermal barrier coatings, yttria-stabilized zirconia (YSZ)

15272648, 2024, 4, Downloaded from https://onlinelibrary.wiley.com/doi/10.1002/adem.202300623 by Forschungszentrum Jülich GmbH Research Center, Wiley Online Library on [11/03/2024]. See the Term

articles are governed by the applicable Creative Commons

www.advancedsciencenews.com

www.aem-journal.com

4DVANCED

Received: May 1, 2023 Revised: June 13, 2023

Published online: June 28, 2023

- [1] S. Stecura, NASA Technical Memorandum 78976, National Aeronautics and Space Administration 1979.
- [2] N. P. Padture, M. Gell, E. H. Jordan, Science 2002, 296, 280.
- [3] R. Vaßen, M. O. Jarligo, T. Steinke, D. E. Mack, D. Stöver, Surf. Coat. Technol. 2010, 205, 938.
- [4] U. Schulz, B. Saruhan, K. Fritscher, C. Levens, Int. J. Appl. Ceram. Technol. 2004, 1, 302.
- [5] E. Bakan, R. Vaßen, J. Therm. Spray Technol. 2017, 26, 992.
- [6] P. Morrell, D. S. Rickerby, papers presented 85th Meeting of the AGARD Structures and Materials Panel, Aalborg, Denmark, 15-16 October 1997, AGARD, Neuilly-sur-Seine, pp. 20-1-20-9.
- [7] B. Bernard, A. Quet, L. Bianchi, A. Joulia, A. Malié, V. Schick, B. Rémy, Surf. Coat. Technol. 2017, 318, 122.
- [8] A. Feuerstein, J. Knapp, T. Taylor, A. Ashary, A. Bolcavage, N. Hitchman, J. Therm. Spray Technol. 2008, 17, 199.
- [9] B. Gillessen, H. Heinrichs, J.-F. Hake, H.-J. Allelein, Appl. Energy 2019, 251, 113377.
- [10] R. Vaßen, D. E. Mack, M. Tandler, Y. J. Sohn, D. Sebold, O. Guillon, J. Am. Ceram. Soc. 2021, 104, 463.
- [11] S. Mihm, PhD Thesis, 2017.
- [12] G. Blandin, R. W. Steinbrecher, PhD Thesis, 2002.
- [13] A. Kulkarni, A. Vaidya, A. Goland, S. Sampath, H. Herman, Mater. Sci. Eng. A 2003, 359, 100.
- [14] M. Ahrens, S. Lampenscherf, R. Vaßen, D. Stöver, J. Therm. Spray Technol. 2004, 13, 432.
- [15] S. Karthikeyan, V. Balasubramanian, R. Rajendran, Ceram. Int. 2014, 40. 3171.
- [16] B. Z. Janos, E. Lugscheider, P. Remer, Surf. Coat. Technol. 1999, 113,
- [17] C. S. Ramachandran, V. Balasubramanian, P. V. Ananthapadmanabhan, Ceram. Int. 2013, 39, 649.

- [18] S. Mahade, A. Venkat, N. Curry, M. Leitner, S. Joshi, Coatings 2021, 11. 86.
- [19] T. Duda, PhD Thesis, Zugl.: Dortmund, Univ., Diss., Mainz, Aachen 2002
- [20] C. S. Ramachandran, V. Balasubramanian, P. V. Ananthapadmanabhan, J. Therm. Spray Technol. 2011, 20, 590.
- [21] S. Karthikeyan, V. Balasubramanian, R. Rajendran, Appl. Surf. Sci. 2014. 296. 31.
- [22] A. Mehta, H. Vasudev, S. Singh, Mater. Today: Proc. 2020, 26, 1336.
- [23] G. E. P. Box, K. B. Wilson, J. R. Stat. Soc. Series B 1951, 13, 38.
- [24] S. Papuga, I. Pećanac, M. Stojković, A. Savić, A. Velemir, Foods Raw Mater. 2022, 10, 137.
- [25] A. I. Khuri, BBIJ 2017, 5, 87.
- [26] M. A. Bezerra, R. E. Santelli, E. P. Oliveira, L. S. Villar, L. A. Escaleira, Talanta 2008, 76, 965.
- [27] G. E. P. Box, D. W. Behnken, Technometrics 1960, 2, 455.
- [28] B. G. Tabachnick, L. S. Fidell, Experimental Designs Using ANOVA, Thomson Brooks/Cole, Belmont, CA 2007.
- [29] R. Darolia, Int. Mater. Rev. 2013, 58, 315.
- [30] J. Chevalier, L. Gremillard, A. V. Virkar, D. R. Clarke, J. Am. Ceram. Soc. 2009 92 1901
- [31] R. Vaßen, E. Bakan, S. Schwartz-Lückge, Coatings 2021, 11, 449.
- [32] P. Fauchais, J. F. Coudert, M. Vardelle, A. Vardelle, A. Denoirjean, Plasma Spraying: Theory And Applications (Ed: R. Suryanarayanan), World Scientific, University of Limoges, France 1993, pp. 61-92.
- [33] K. Ramachandran, J.-L. Marqués, R. Vaßen, D. Stöver, J. Phys. D: Appl. Phys. 2006, 39, 3323.
- [34] M. Vardelle, A. Vardelle, P. Fauchais, M. I. Boulos, AIChE J. 1983, 29, 236.
- [35] G. Montavon, C. Coddet, S. Sampath, H. Herman, C. C. Berndt, J. Therm. Spray Technol. **1997**, 6, 153.
- [36] C. S. Ramachandran, V. Balasubramanian, P. V. Ananthapadmanabhan, Surf. Eng. 2011, 27, 217.
- [37] A. K. Ray, R. W. Steinbrech, J. Eur. Ceram. Soc. 1999, 19, 2097.
- [38] G.-R. Li, G.-J. Yang, C.-X. Li, C.-J. Li, Ceram. Int. 2018, 44, 2982.
- [39] R. S. Lima, Coatings 2020, 10, 812.